

Unconstrained shape optimisation of singly-symmetric and open cold-formed steel beams and beam-columns



Bin Wang^{a,*}, Guillaume L. Bosco^a, Benoit P. Gilbert^a, Hong Guan^a, Lip H. Teh^b

^a Griffith School of Engineering, Gold Coast Campus, Griffith University, QLD 4222, Australia

^b School of Civil, Mining and Environmental Engineering, University of Wollongong, NSW 2522, Australia

ARTICLE INFO

Article history:

Received 27 November 2015

Received in revised form

23 February 2016

Accepted 5 March 2016

Keywords:

Shape optimisation

Cold-formed steel structures

Beams

Beam-columns

Genetic Algorithm

ABSTRACT

This study aims to optimise the cross-sectional shape of singly-symmetric, open-section and simply-supported cold-formed steel (CFS) beams and beam-columns. No manufacturing or assembly constraints are considered. The previously developed augmented Lagrangian Genetic Algorithm (GA), referred to as the “self-shape” optimisation algorithm, is used herein. Fully restrained and unrestrained beams against lateral deflection and twist, as well as unrestrained beam-columns are optimised. Various combinations of axial compressive load and bending moment are analysed for the beam-columns. The Direct Strength Method (DSM) is used to evaluate the nominal member compressive and bending capacities. The accuracy of the automated rules, developed in the literature to determine the elastic local and distortional axial buckling stresses from Finite Strip signature curves, is verified herein to estimate the elastic bending buckling stresses. The optimised cross-sectional shapes are presented for all cases and the evolution of the unrestrained shapes from pure axial compression to pure bending is discussed.

© 2016 Elsevier Ltd. All rights reserved.

1. Introduction

Cold-formed steel (CFS) members are intensively used in the construction industry due to their ease of erection and low weight-to-capacity ratio [1]. Their structural efficiency lies in the versatility of the cross-sectional shapes that enhances the strength by controlling the three fundamental buckling modes, i.e. local, distortional and global. Local buckling is enhanced in practice by adding wall stiffeners, while lip stiffeners and rear flanges greatly influence distortional buckling [2].

Improving the overall cross-sectional shape of CFS members through shape optimisation algorithms is currently gaining significant interest. The ultimate objective is to discover new and innovative optimum cross-sections that can be manufactured and practicably used onsite.

Nevertheless, research on shape optimisation of CFS members has been solely restricted to columns with unconstrained (where the algorithm is free to converge to any cross-sectional shapes) [3–7] and constrained (where sections are able to be manufactured and/or practicably assembled onsite) [8–12] problems. Shape optimisation of CFS beams has been seldom investigated and the optimisation of CFS beams has been primarily performed so far by algorithms that aimed at optimising the dimensions of a given

cross-section rather than optimising the cross-sectional shape itself, see [13–17] for instance. Shape optimisation of thin-walled beams has been performed to a certain extent [18,19], but only to maximise the second moments of area and minimise the cross-sectional area.

This paper aims at shape optimising the cross-sections of unconstrained (no manufacturing and assembly constraints) CFS beams and beam-columns by minimising their cross-sectional area for various combinations of axial compressive load and bending moment. Unconstrained optimisation problems allow the “absolute” optimised cross-sectional shape to be discovered. This outcome provides a reference shape to be compared to when manufacturing and assembly constraints are later introduced into the algorithm. The present work is therefore an important step in shape optimisation of practical CFS sections. An existing shape optimisation algorithm [4,18] is used for this purpose.

The Direct Strength Method (DSM) [20] is used to calculate the nominal axial compressive and bending capacities of the cross-sections. Rules to automatically estimate the elastic bending local and distortional buckling stresses to be used in the DSM are given and verified against 64 cross-sections. The algorithm is applied to beams that are either restrained (braced) or not against lateral deflection and twist, and unrestrained (unbraced) beam-columns. The optimised cross-sectional shapes are presented and the evolution of the unrestrained shapes from pure axial compression to pure bending is discussed.

* Corresponding author.

E-mail address: b.wang@griffith.edu.au (B. Wang).

2. The shape-optimisation algorithm

In this study, the “self-shape” optimisation algorithm for CFS members, for which the principles are published in [18] and its applications to singly-symmetric cross-sections are presented in [4], is used. Genetic Algorithm (GA) [21] is used as the search algorithm. The GA is combined with the Augmented Lagrangian (AL) method [22] to avoid ill-conditioned processes by ensuring finite values of the penalty factors.

Initial cross-sections are drawn using self-avoiding random walks. Cross-over and mutation operators are performed on a design space [4,18]. The algorithm has the advantages of (i) being verified against a known optimisation problem for which an analytical solution exists [18] and (ii) allowing arbitrary cross-sections to be initially created with no presumption of the optimised shape. Examples of arbitrary drawn singly-symmetric and open cross-sections in the initial population can be found in [4].

More information and full details of the algorithm are available elsewhere [4, 18]. The calibration of the factors used in the AL method is given in [18].

3. The optimisation problem

The “self-shape” optimisation algorithm is used herein to optimise simply-supported, free-to-warp, singly-symmetric and open-section beams and beam-columns. The three fundamental buckling modes, i.e. local, distortional and global, are incorporated through the use of the DSM, as described in Section 4. The yield stress f_y of the steel is 450 MPa, the Young’s modulus E is 200 GPa and the shear modulus G is 80 GPa. The wall thickness t is taken as 1.2 mm. The member is subjected to a uniform bending moment M^* about its axis of symmetry (x -axis) and a compressive axial load N^* . The optimisation problem is illustrated in Fig. 1.

In reference to Fig. 1, the member length L is fixed throughout this paper at 1.5 m. Five load cases (LC) are considered to investigate the optimum cross-sectional shapes of simply supported beams, columns and beam-columns:

- LC1: Pure bending ($N^*=0$ and $M^*=2.5$ kN m) for a fully restrained beam, (i.e. $L_{ey}=L_{ez}=0$ m, where L_{ey} and L_{ez} are the effective buckling lengths for bending about the y -axis and for twisting about the longitudinal z -axis, respectively).
- LC2: Same moment as LC1 but for an unrestrained beam (i.e. $L_{ey}=L_{ez}=L=1.5$ m).
- LC3: Pure axial compression ($N^*=75$ kN and $M^*=0$) for an unrestrained column (i.e. $L_{ex}=L_{ey}=L_{ez}=L=1.5$ m, where L_{ex} is the effective buckling length for bending about the axis of symmetry). This case has already been investigated in [12] and the previously obtained results are used in this study.
- LC4: Combined actions for an unrestrained beam-column with dominant bending. N^* is taken as $1/3$ of the axial compressive load in LC3 and M^* as $2/3$ of the bending moment in LC2 ($N^*=25$ kN and $M^*=1.67$ kN m).
- LC5: Combined actions for an unrestrained beam-column with dominant axial compression. N^* is taken as $2/3$ of the axial compressive load in LC3 and M^* as $1/3$ of the bending moment in LC2 ($N^*=50$ kN and $M^*=0.83$ kN m).

As cold-rolled steel coil can usually be ordered in any width, the approach is to mimic a CFS manufacturer who wants to optimise the cross-sectional shape against a given design loading combination. The unconstrained problem in the GA consists of minimising the cross-sectional area A_s subject to an inequality penalty function on N^* and M^* . The interaction equation described in Clause 3.5 of the Australian cold-formed steel design

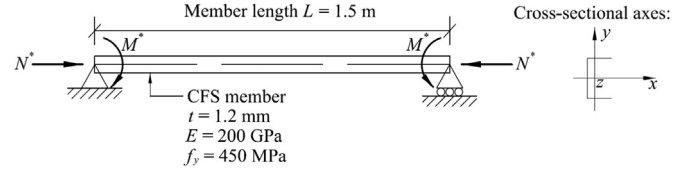


Fig. 1. Optimisation problem.

specification AS/NZS 4600 [23] is used as the penalty function,

$$\frac{N^*}{\phi_c N_c} + \frac{M^*}{\phi_b M_b} \leq 1 \quad (1)$$

where ϕ_c and ϕ_b are capacity reduction factors, taken as 1.0 in this study. N_c and M_b are the nominal member compressive and bending capacities of the cross-section, respectively. The general form of the fitness function f suitable for GA is then expressed as,

$$f = \frac{A_s}{A_{ref}} + \alpha \left\{ \max \left[0, \left(\frac{N^*}{N_c} + \frac{M^*}{M_b} - 1 \right) \right] \right\} \quad (2)$$

where A_{ref} is the reference area of similar value to the optimised cross-sectional area. A_{ref} is estimated herein with preliminary runs and is taken as 190 mm² for LC1, 292 mm² for LC3 [12], and 260 mm² for other cases. α is a penalty factor [21].

To avoid ill-conditioning problem, the AL constraint-handling method developed in [22] for the GA is used. The actual form of the fitness function f used in the algorithm then becomes,

$$f = \frac{A_s}{A_{ref}} + \frac{1}{2} \left\{ \gamma \left[\max \left(0, \left(\frac{N^*}{N_c} + \frac{M^*}{M_b} - 1 \right) + \mu \right) \right]^2 \right\} \quad (3)$$

where γ is the penalty function coefficient, and μ is the real parameter associated with the penalty function. Initial values of $\gamma=2.0$ and $\mu=0$ found in [18] are used. Similar to [18], the AL penalty increasing constant β and convergence rate ρ are set to 1.05 and 1.5, respectively.

Detailed parameters of the GA used in this paper are given in [4,18]. In this study, 500 cross-sections are analysed per generation and the algorithm converges in less than 60 generations (see Section 5.1). Therefore, a maximum of 30,000 solutions in total are analysed per run, this is similar to the 40,000 solutions analysed per run in [7]. 10 runs are performed for each load case to verify the robustness of the algorithm. The design space is set to 100 mm × 100 mm. The cross-sections are composed of consecutive elements having nominal length of 4 mm. The probabilities of cross-over and mutation operators are equal to 80% and 1%, respectively.

4. Nominal member compressive and moment capacities

4.1. The Direct Strength Method (DSM)

The DSM [20] allows designing CFS members for local, distortional and global buckling simultaneously. The method presents the same degree of complexity for any cross-sectional shapes and therefore is well suited for shape optimisation problems. The DSM as published in Clauses 7.2.1 and 7.2.2 of the AS/NZS 4600 [23] is used in this study to calculate the nominal member compressive and moment capacities N_c and M_b , respectively. N_c is expressed as,

$$N_c = \min(N_{ce}, N_{cl}, N_{cd}) \quad (4)$$

where N_{ce} , N_{cl} and N_{cd} are the nominal member capacities in compression for global, local and distortional buckling, respectively. Similarly, M_b is expressed as,

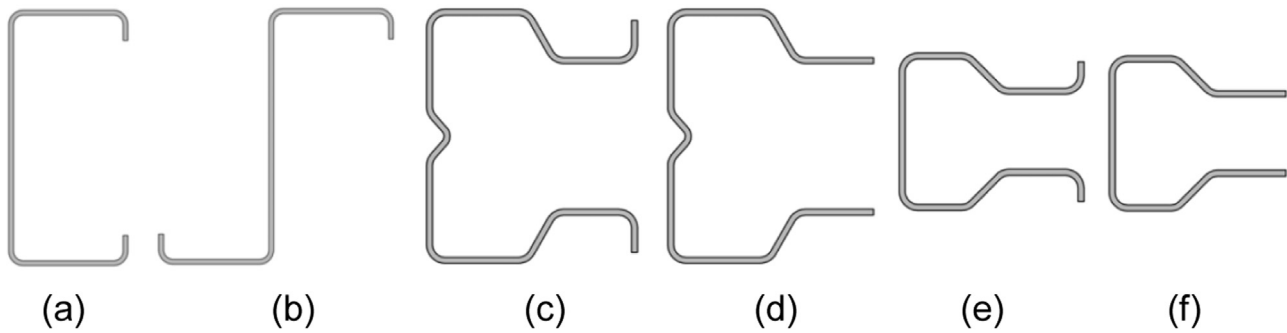


Fig. 2. Cross-sections, (a) “Cee” and (b) “Zed”, storage rack uprights (c) with web and lip stiffeners, (d) with web stiffener only, (e) with lip stiffener only, and (f) without web and lip stiffeners.

$$M_b = \min(M_{be}, M_{bl}, M_{bd}) \quad (5)$$

where M_{be} , M_{bl} and M_{bd} are the nominal member moment capacities for global, local and distortional buckling, respectively. The DSM is well developed in the literature and the references to [20,23] are made for instance.

4.2. Elastic buckling stresses

4.2.1. Determining elastic buckling stresses

The local and distortional elastic buckling stresses f_{ol} and f_{od} in pure compression and bending, respectively, needed in the DSM to determine the local and distortional nominal member capacities are estimated herein by performing Finite Strip analyses [24] using the open source software CUFSM [25]. CUFSM was incorporated into the algorithm in [4]. The global elastic member buckling load N_{oc} and buckling moment M_o needed to determine the global nominal capacities (N_{ce} and M_{be}) are calculated in accordance with the Equations given in Clauses 3.4.3 and 3.3.3.2.1 (a) of the AS/NZS 4600 [23], respectively. In the best case scenario, the signature curves produced by the Finite Strip Method (FSM) [24] have two distinct local minima representing the elastic local buckling stress f_{ol} (first minimum) and the elastic distortional buckling stress f_{od} (second minimum). Nevertheless, the FSM often generates indistinct buckling modes with none, one or more than two local minima. In such cases, the elastic buckling stresses need to be “manually” identified using engineering judgement [26]. As manual methods are not compatible with optimisation algorithms, rules to automatically detect the elastic local and distortional buckling stresses from the signature curves have been developed in [4]. However, these rules have only been verified so far for elastic axial buckling stresses and need to be further verified for elastic bending buckling stresses. The rules are as follows (see [4] for more details and the underlining philosophy):

- For the elastic local buckling stress f_{ol} :
 - Step 1: Calculate the signature curve in CUFSM using the FSM in the half-wavelength interval $[r_o, d]$ where r_o is the least radius of gyration and d is the largest overall dimension of the cross-section.
 - Step 2: a) If at least one local minimum exists in the interval, then f_{ol} is taken as the smallest local minimum;
 - Else, f_{ol} is taken as the minimum gradient of the signature curve in the interval.
- For the elastic distortional buckling stress f_{od} :

Step 1: a) Calculate the pure distortional signature curve using the constrained Finite Strip Method (cFSM) [27] in CUFSM in the half-wavelength interval $[\min(20r_o, 3d), 10d]$;

b) If at least one local minimum exists in the interval, then record the critical half-wavelength L_{crd} corresponding to the

minimum value on the curve between the smallest local minimum and the values at the bounds of the interval, and go to Step 3;

c) Else, go to Step 2.

Step 2: Expand the upper limit of the interval by $3d$ and run the pure distortional signature curve in the new interval using the cFSM module and go to Step 1 b).

Step 3: Calculate f_{od} from the signature curve using the FSM at the half-wavelength L_{crd} .

4.2.2. Rules validation for elastic bending buckling stresses

The automated rules in Section 4.2.1 are validated herein for elastic bending buckling stresses against the manual method described in Clause 3.3 of the Direct Strength Method Design Guide [26]. Specifically, to handle an indistinct local mode, the basic options include: (i) refining the half-wavelength steps, (ii) basing judgement on the local buckling mode definition, (iii) pinning internal fold lines to force local buckling if possible, or (iv) conservatively choosing the lowest elastic buckling stress at a half-wavelength less than d . Similarly, the options to handle an indistinct distortional mode involve: (i) refining the half-wavelength steps, (ii) basing judgement on the distortional buckling mode definition, (iii) pinning internal fold lines to isolate local buckling from distortional buckling if possible, (iv) slightly altering the dimensions of the cross-section to detect a trend in the distortional buckling minima, or (v) conservatively selecting the lowest buckling mode which exhibits the distortional buckling features at a half-wavelength greater than the local buckling half-wavelength.

The same forty-eight conventional cross-sections (sixteen “Cee” and sixteen “Zed” sections from BlueScope Lysaght [28] and sixteen storage rack uprights) used to validate the automated rules for elastic axial buckling stresses in [4] and sixteen optimised beam and beam-column sections obtained in the next section are used herein to validate the automated rules for elastic bending buckling stresses. The conventional sections are shown in Fig. 2 and the exact dimensions are given in [29]. Table 1 lists the differences between the automated rules and the manual method for both local and distortional buckling stresses. The automated rules are accurate with an average error of 0.01% and 0.33% for local and distortional buckling, respectively. The automated rules usually provide lower elastic buckling stresses (conservative) than the manual method. The maximum difference between the two methods is found for a 110 mm deep and 1.2 mm thick rack upright section with lip stiffeners, being 6.59%.

The signature curves, together with the deformed buckling shapes, of the fittest optimised section for LC1 are shown in Fig. 3. The cross-section is an “I” type (see Section 5 for more details) and distortional buckling does not occur. The manual method would therefore not consider distortional buckling in the DSM while the automated rules predict distortional buckling at a half-wavelength of 58 mm in Fig. 3. Therefore, by calculating the distortional

Table 1
Comparison of elastic buckling stresses between automatic rules and manual method.

Section types	No. of sections analysed	Depth to thickness ratio		Difference in elastic buckling stresses between automatic rules and manual method (%) ^a					
		Min	Max	Local		Distortional			
				Average	Min	Max	Average	Min	Max
“Cee”	16	52.6	133.3	0.02	0.00	0.21	0.00	0.00	0.00
“Zed”	16	52.6	133.3	0.02	0.00	0.18	1.89	0.00	6.58
Upright (lips)	9	22.9	60.0	0.01	0.00	0.04	-1.02	-3.63	6.59
Upright (no lips)	7	22.9	60.0	0.00	0.00	0.00	0.00	0.00	0.00
Optimum (LC1)	4	100.3	103.1	0.00	0.00	0.00	-	-	-
Optimum (LC2)	4	79.5	82.5	0.00	0.00	0.00	0.00	0.00	0.00
Optimum (LC4)	4	88.4	98.5	0.00	0.00	0.00	0.00	0.00	0.00
Optimum (LC5)	4	75.8	88.8	0.00	0.00	0.00	0.00	0.00	0.00
All sections	64	22.9	133.3	0.01	-	-	0.33	-	-

^a A negative percentage value means that the elastic buckling stress from the automated rules is higher than that from the manual method.

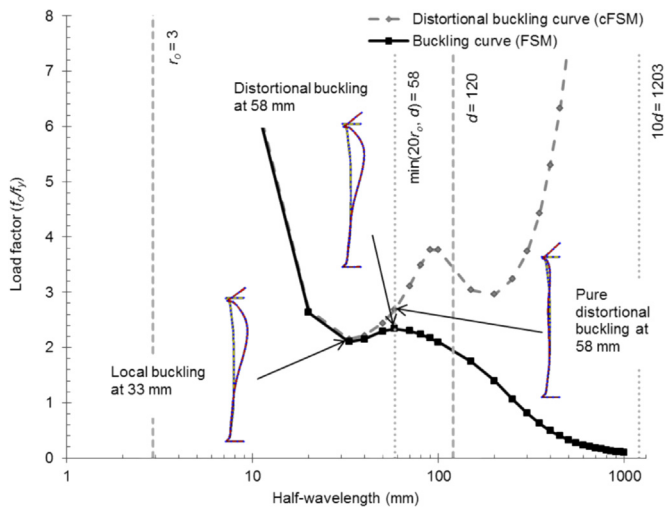


Fig. 3. Buckling curves for the fittest cross-section in LC1.

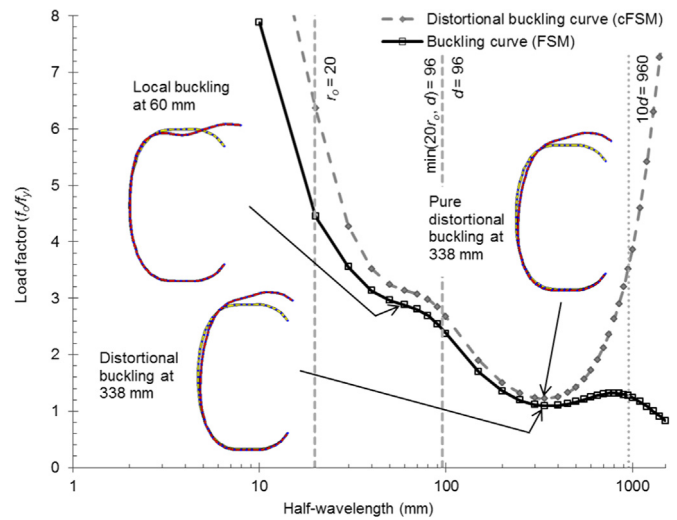


Fig. 4. Buckling curves for the fittest cross-section in LC2.

nominal member moment capacity M_{bd} , the automated rules lead to conservative results. It is worth mentioning that the calculated M_{bd} is always equal to the moment causing initial yield at the extreme compression fibre M_y for all optimised sections for LC1. Local buckling is captured by the two methods at a half-wavelength of 33 mm.

The signature curves of the fittest optimised section for LC2 are shown in Fig. 4. The signature curves of the optimised sections for LC3 and LC5 present similarity to Fig. 4. One local minimum gradient is found at 60 mm on the FSM curve and is selected by both methods to predict the local elastic buckling stress. A local minimum at 338 mm is observed for the distortional buckling mode and is therefore selected by the manual method. The pure distortional buckling cFSM signature also presents a local minimum at 338 mm leading to the manual and automated rules selecting the same elastic distortional buckling stress.

5. Results and discussion

5.1. Convergence

Fig. 5 shows the average general fitness functions f in Eq. (2), with $\alpha=10$, times A_{ref}/A_s over 10 runs and for all load cases. The coefficient $\alpha=10$ is used to better visualise the convergence by increasing the weight of the constraint. The ratio A_{ref}/A_s , where A_s is the optimised cross-sectional area reported in Section 5.2, enables comparisons of the convergence performance among the five

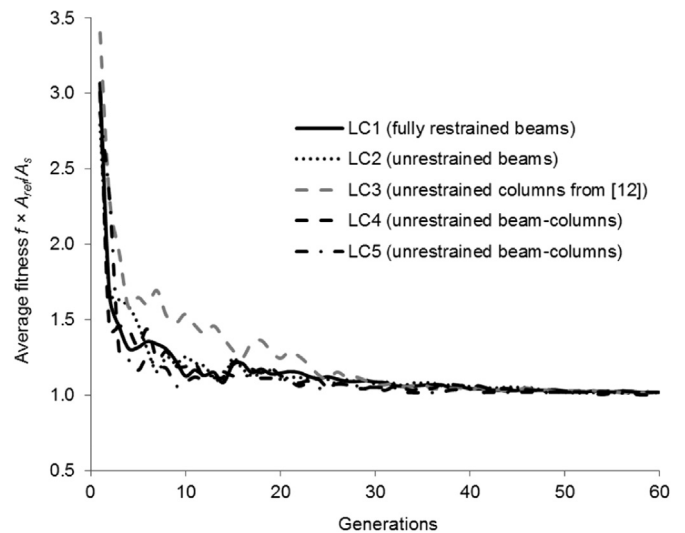


Fig. 5. Average fitness f times A_{ref}/A_s over 10 runs.

load cases. The algorithm always converges to an optimised solution for all load cases in about 50 generations. The convergence rates of beams and beam-columns are similar to each other.

The computation time is highly related to the number of cross-sectional elements in CUFSM [25], written in MATLAB, to perform the Finite Strip analyses. The more the number of elements, the

Table 2
Average results over 10 runs for all load cases.

Load cases	Cross-sectional area		Nominal member capacity in compression			Nominal member moment capacity			Combined Capacity ratio	
	A_s (mm ²)	CoV (%)	N_c (kN)	N'/N_c	CoV (%)	M_b (kN m)	M'/M_b	CoV (%)	$N'/N_c + M'/M_b$	CoV (%)
LC1	189.2	0.19	–	–	–	2.50	1.00	0.39	–	–
LC2	235.2	0.18	–	–	–	2.50	1.00	0.42	–	–
LC3 [12]	289.1	0.31	75.01	1.00	0.05	–	–	–	–	–
LC4	264.4	0.34	55.40	0.45	2.94	3.04	0.55	2.47	1.00	0.38
LC5	281.8	0.33	68.77	0.73	2.20	3.10	0.27	6.49	1.00	0.36

longer the computation time is. Up to 8 computer cores are selected per MATLAB analysis in a 792 core HPC cluster consisting of a mixture of SGI Altix XE and SGI® Rackable™ C2114-4TY14 servers for this purpose. The Finite Strip analyses took about 80% of the total optimisation time. The main algorithm is written in Python and does not use parallel processing.

The average computation time per generation is 40 min for fully restrained beams (LC1), 45 minutes for unrestrained beams (LC2) and 50 minutes for columns (LC3). For the beam-columns, the elastic buckling analyses in CUFSM are run for both the axial compression and bending moment. This considerably slows down the algorithm, and the average computation time per generation reaches 130 minutes for LC4 and 140 minutes for LC5.

5.2. Average results

Table 2 summarises the average results over 10 runs for all load cases. The algorithm always satisfies the strength ratio criteria and converges to consistent solutions with small CoVs on the cross-sectional area (maximum of 0.34% for LC4). This outlines the robustness of the algorithm. For LC1 and LC2 (pure bending), the average nominal member moment capacity M_b is always equal to the target bending moment $M' = 2.5$ kN m with a maximum CoV of 0.42% for LC2. The average optimised cross-sectional area ($A_s = 189.2$ mm²) of the fully restrained beams for LC1 is about 20% smaller than the same of the unrestrained beams for LC2 ($A_s = 235.2$ mm²). For the beam-columns (LC4 and LC5), the interaction equation in Eq. (1) provides an average action-to-capacity ratio of 1.00 with a maximum CoV of 0.38% for LC4.

5.3. Cross-sectional shapes

5.3.1. Fully restrained beams

Fig. 6 illustrates the two fittest (Fig. 6(a) and (b)) and two least fit (Fig. 6(c) and (d)) optimised cross-sectional shapes for the fully restrained beams (LC1). The optimised cross-sectional area A_s is used to determine how fit a cross-section is. As seen in Fig. 6, the fully restrained beams converge to a slender “I” section type with a curved web. The parallel flanges are short and without lip stiffeners. The curved web enhances the local buckling capacity of the web and allows maximising the second moment of area by moving the material away from the neutral axis. “I” sections were already found to be the optimised cross-sectional shape for beams by Griffiths and Miles [30] where only maximising the second moment of area was considered. The slender web may fail under shear and the DSM for shear buckling [31,32] will need to be introduced into the algorithm. The fittest solution in Fig. 6(a) is 120.3 mm deep, 17.1 mm wide and therefore has a depth-to-width ratio of 7.0.

5.3.2. Unrestrained beams

Fig. 7(a)–(d) shows the two fittest and two least fit cross-sections for the unrestrained beams (LC2). Compared to the fully restrained beams with the slender cross-sectional shapes in Fig. 6, the unrestrained beams converge to a largely open and stocky “Cee” section type in Fig. 7. When compared to the restrained beam, this shape allows significantly larger (i) second moment of area about the y-axis that therefore enhances the flexural buckling load about this axis and (ii) warping constant that therefore enhances the torsional buckling load. The difference in torsional constant between the two sections is about 20%. The web is more

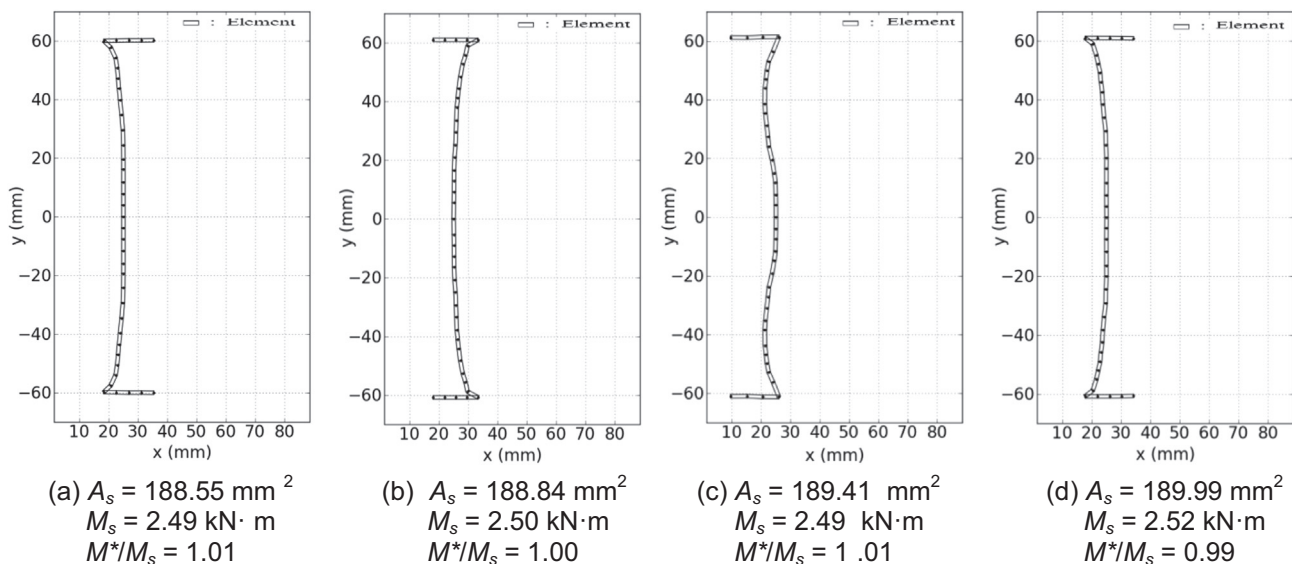


Fig. 6. Optimised cross-sections for LC1, (a, b) fittest and (c, d) least fit cross-sections.

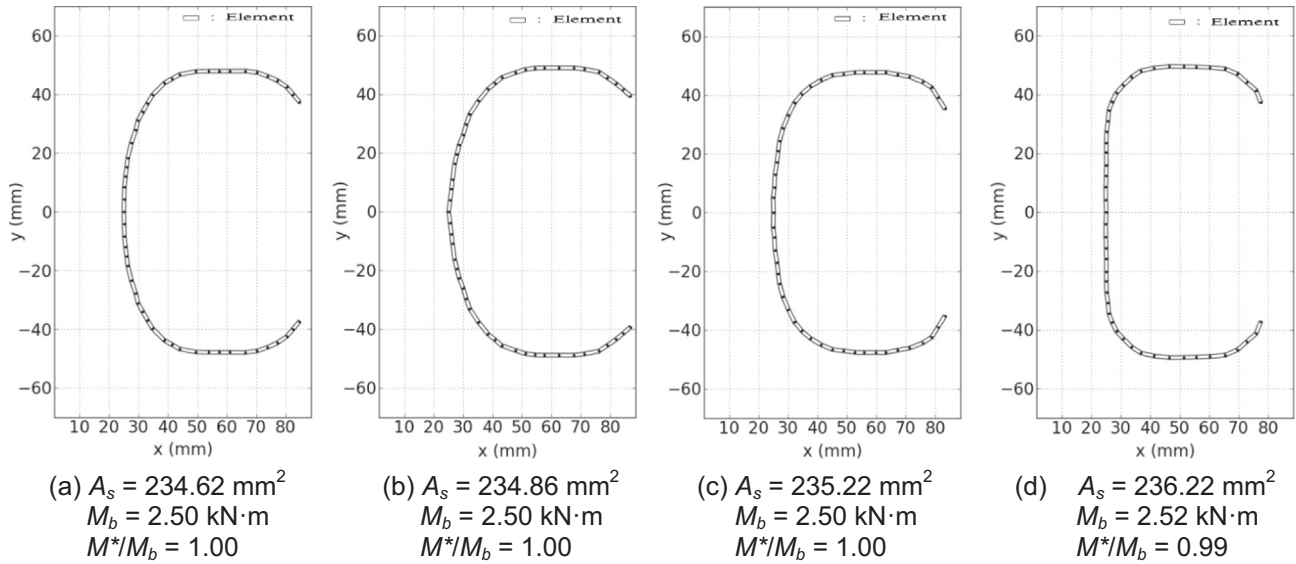


Fig. 7. Optimised cross-sections for LC2, (a, b) fittest and (c, d) least fit cross-sections.

rounded for the two fittest cross-sections in Fig. 7(a) and (b) than the two least fit ones in Fig. 7(c) and (d). All cross-sections in Fig. 7 have short lip stiffeners of about 18 mm, approximately orientated at 45° to the horizontal flange. The depth of the fittest section in Fig. 7(a) is 95.9 mm, the width is 59.6 mm, and therefore the depth-to-width ratio is 1.6. This corresponds to a depth-to-width ratio 77% less than the fittest cross-section in Fig. 6(a).

5.3.3. Unrestrained columns

Fig. 8 presents for reference the two fittest and two least fit cross-sections for the 1.5 m long columns in [12]. These cross-sections are typically rounded and close, especially for the fittest ones. The fittest cross-section in Fig. 8(a) has a depth of 93.3 mm, a width of 50.6 mm and therefore a depth-to-width ratio of 1.8, similar to the fittest one of the unrestrained beams in Fig. 7(a).

5.3.4. Unrestrained beam-columns

Fig. 9 and Fig. 10 show the two fittest and two least fit cross-sections for LC4 and LC5, respectively. In Fig. 9(a)–(c), an open “Cee” section type with curved lip stiffeners, approximately orientated at 45° to the flange, is found, whereas in Fig. 9(d) a largely open “Sigma” type cross-sectional shape with short curved lip stiffeners is found. The lip stiffeners in Fig. 9(a)–(c) are about

25 mm longer than the ones of the unrestrained beams in Fig. 7 and the cross-sectional shapes are less open.

When the design axial load N^* increases and the design bending moment M^* decreases in LC5, the cross-sections in Fig. 10 tend to close up more than the ones in Fig. 9 (LC4). The cross-sections also tend to resemble those of the columns in Fig. 8. The cross-sectional shapes in Fig. 10 (LC5) are therefore stockier than the ones in Fig. 9 (LC4). The fittest solution in Fig. 10 (a) has a depth of 101.1 mm, a width of 49.4 mm and thus a depth-to-width ratio of 2.1, i.e. about the same width as the fittest cross-section for LC4 but 8.6% shorter. The fittest cross-sectional area $A_s=280.75 \text{ mm}^2$ in Fig. 10 (a) is 6.3% larger than the one in Fig. 9(a).

While Fig. 10 (c) and (d) have similar cross-sectional areas (within 0.1%) and interaction ratios (Eq. (1)), they adopt different strategies to satisfy the strength requirement. The cross-section in Fig. 10 (c) has a depth-to-width ratio of 1.9 and is nearly closed, while the cross-section in Fig. 10 (d) is 14.6% deeper and 11.5% wider, with a depth-to-width ratio of 2.0, but open. This derives from the cross-section in Fig. 10 (c) favouring its nominal axial capacity N_c instead of its nominal bending capacity M_b ($N_c=71.50 \text{ kN}$ and $M_b=2.77 \text{ kN m}$) to decrease the action-to-capacity ratio in Eq. (1) and the cross-section in Fig. 10 (d) ($N_c=68.86$ and $M_b=3.13 \text{ kN m}$) favouring the opposite. The cross-section in

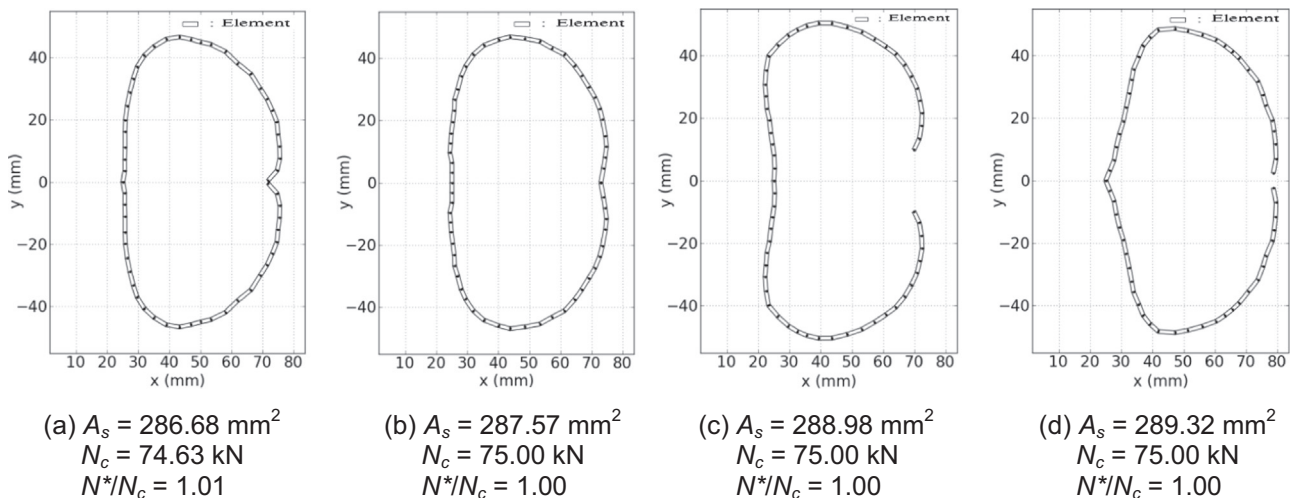


Fig. 8. Optimised cross-sections for LC3 (from [12]), (a, b) fittest and (c, d) least fit cross-sections.

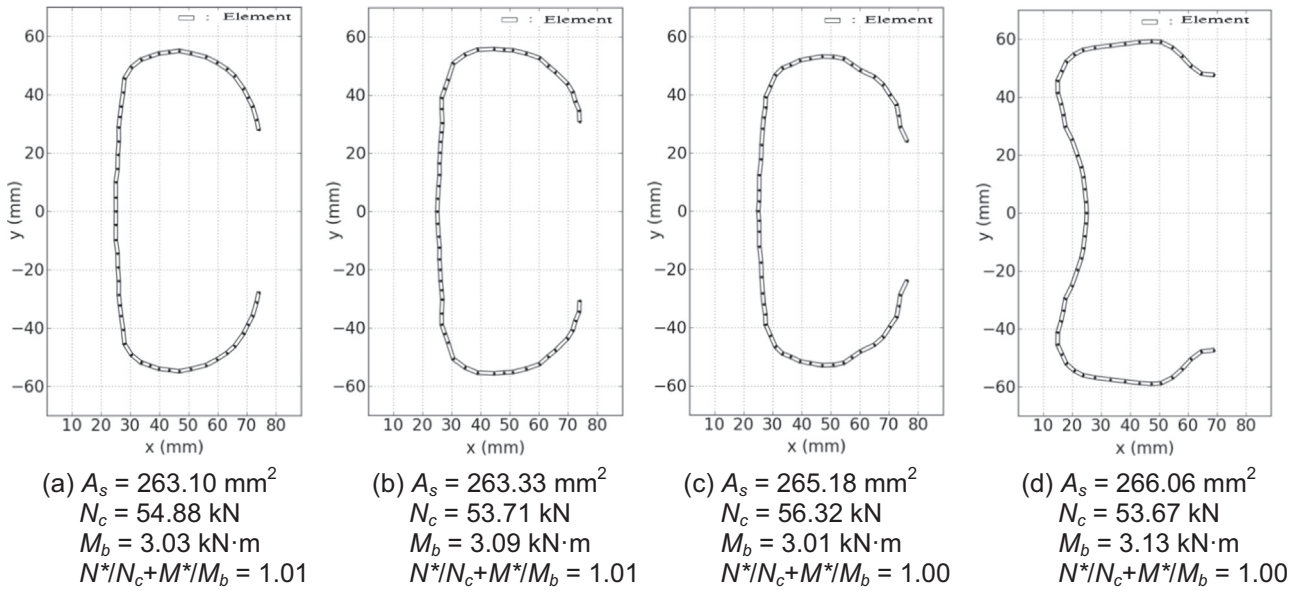


Fig. 9. Optimised cross-sections for LC4, (a, b) fittest and (c, d) least fit cross-sections.

Fig. 10 (c) therefore resembles more to the optimised columns in Fig. 8 (LC3) while the one in Fig. 10 (d) resembles more to the optimised beam-columns in Fig. 9 (LC4).

5.4. Evolution of the optimised cross-section from column to beam

The evolution of the average results (see Section 5.2) and the fittest shape (see Section 5.3) for the unrestrained cases is summarised in Fig. 11. As the design bending moment M^* increases from zero to 2.5 kN m and the design axial compression N^* decreases from 75 kN to zero, the average cross-sectional area A_s decreases by 18.6% from 289.1 to 235.2 mm² and the fittest cross-sectional shape gradually opens up as described in Section 5.3. Specifically, the cross-sectional area only decreases by 2.5% between LC3 and LC5 where the design axial load N^* decreases by 33%. This result implies that the value of the design moment ($M^* = 0.83 \text{ kN m}$) in LC5 is not large enough to significantly influence the cross-sectional shape. However, the reduction in the cross-

sectional area increases to 6.3% when the design axial load N^* is further reduced from 50 kN to 25 kN between LC5 and LC4, and to 10.8% between LC4 and LC2 when N^* is reduced from 25 kN to zero.

6. Conclusions

This paper aims to optimise the cross-sectional shapes of CFS beams and beam-columns. Manufacturing and assembly constraints were not included in this study. Various load combinations of axial compressive load and bending moment were used to perform shape optimisations of simply-supported 1.5 m long singly-symmetric sections. Fully restrained beams and unrestrained beams and beam-columns against lateral deflection and twist were considered. The rules to automatically determine the elastic local and distortional buckling stresses from the Finite Strip Method signature curve developed in [4] were verified for elastic

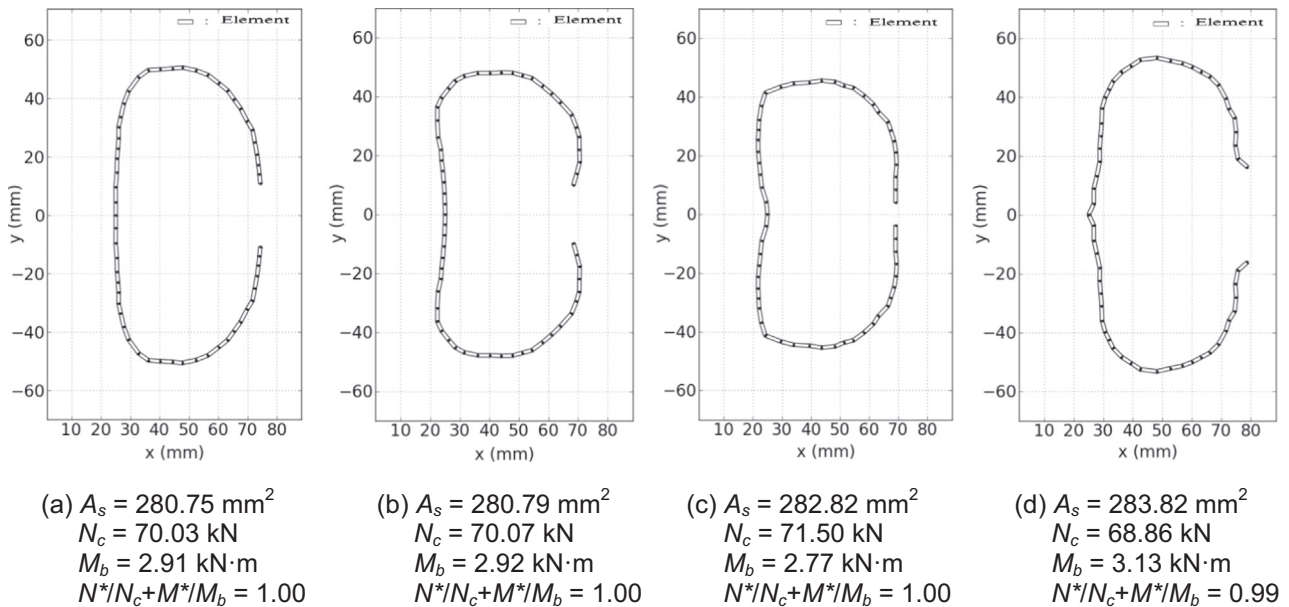
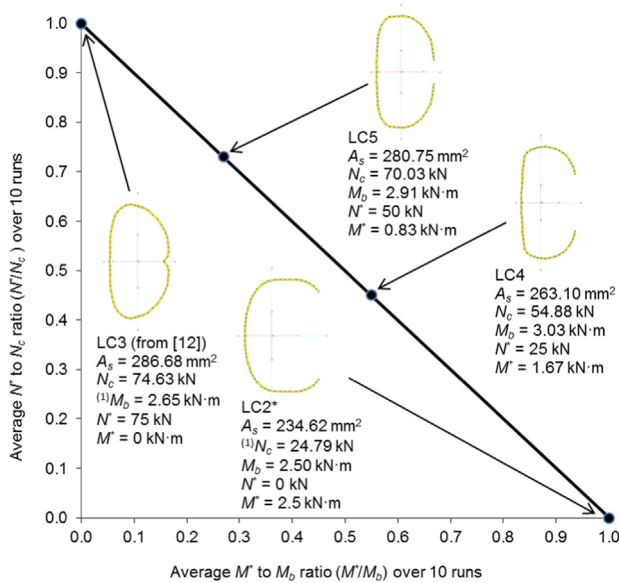


Fig. 10. Optimised cross-sections for LC5, (a, b) fittest and (c, d) least fit cross-sections.



(1) The nominal axial compressive and bending capacities N_c and M_b for the cross-sections in LC2 and LC3 are calculated by hand, respectively.

Fig. 11. Evolution of average cross-sectional areas and shapes for the unrestrained load cases.

bending buckling stresses. The main conclusions can be summarised as follows:

- The robustness of the algorithm is demonstrated by consistent optimised solutions over 10 runs.
- The automated rules were found to accurately determine the elastic local and distortional bending buckling stresses.
- The algorithm was able to converge to optimised cross-sectional shapes of CFS members subject to pure bending and combined axial compression and bending.
- An optimised slim “I” type cross-sectional shape with a curved web was typically found for the fully restrained beams, and a stocky and largely open “Cee” like cross-sectional shape with lip stiffeners for the unrestrained beams. For the unrestrained beam-columns, “Cee” type cross-sectional shapes were also found, with the cross-section tending to close up when the axial compressive load was increased and to open up when the bending moment was increased.
- The unconstrained algorithm for shape optimisation of CFS beams or beam-columns allows the cross-section able to freely converge to any cross-sectional shape. This gives a reference cross-sectional shape for the constrained one with manufacturing and assembly constraints found in the future.

References

- [1] G.J. Hancock, Design of cold-formed steel structures (to AS/NZ 4600:2007) – 4th Edition, Australian Steel Institute, North Sydney, Australia, 2007.
- [2] G.J. Hancock, Distortional buckling of steel storage rack columns, *J. Struct. Eng.* (1985).
- [3] H. Liu, T. Igusa, B. Schafer, Knowledge-based global optimization of cold-formed steel columns, *Thin-Walled Struct.* 42 (2004) 785–801.
- [4] B.P. Gilbert, T.J.M. Savoyat, L.H. Teh, Self-shape optimisation application: Optimisation of cold-formed steel columns, *Thin-Walled Struct.* 60 (2012) 173–184.
- [5] J. Leng, J.K. Guest, B.W. Schafer, Shape optimization of cold-formed steel columns, *Thin-Walled Struct.* 49 (2011) 1492–1503.
- [6] M. Moharrami, A. Louhghalam, M. Tootkaboni, Optimal folding of cold formed steel cross sections under compression, *Thin-Walled Struct.* 76 (2014) 145–156.
- [7] J.F.A. Madeira, J. Dias, N. Silvestre, Multiobjective optimization of cold-formed steel columns, *Thin-Walled Struct.* 96 (2015) 29–38.
- [8] J. Leng, Z. Li, J.K. Guest, B.W. Schafer, Constrained shape optimization of cold-formed steel columns, in: Proceedings of the 21st International Specialty Conference on Cold-Formed Steel Structures, St. Louis, MO, United States, 2012, pp. 9–73.
- [9] J. Leng, Z. Li, J.K. Guest, B.W. Schafer, Shape optimization of cold-formed steel columns with manufacturing constraints and limited number of rollers, in: Proceedings of the Structural Stability Research Council Annual Stability Conference, 2013, pp. 313–331.
- [10] J. Leng, Z. Li, J.K. Guest, B.W. Schafer, Shape optimization of cold-formed steel columns with fabrication and geometric end-use constraints, *Thin-Walled Struct.* 85 (2014) 271–290.
- [11] J.M.S. Franco, J.P. Duarte, Ed.M. Batista, A. Landesmann, Shape grammar of steel cold-formed sections based on manufacturing rules, *Thin-Walled Struct.* 79 (2014) 218–232.
- [12] B. Wang, B.P. Gilbert, A.M. Molinier, H. Guan, L.H. Teh, Shape optimisation of cold-formed steel columns with manufacturing constraints using the Hough transform, *Thin-Walled Struct.* (2015) (Submitted for publication).
- [13] H. Adeli, A. Karim, Neural network model for optimization of cold-formed steel beams, *J. Struct. Eng.* 123 (1997) 1535–1543.
- [14] A. Karim, H. Adeli, Global optimum design of cold-formed steel hat-shape beams, *Thin-Walled Struct.* 35 (1999) 275–288.
- [15] J. Lee, S.-M. Kim, H.-S. Park, B.-H. Woo, Optimum design of cold-formed steel channel beams using micro Genetic Algorithm, *Eng. Struct.* 27 (2005) 17–24.
- [16] T. Tran, L.-Y. Li, Global optimization of cold-formed steel channel sections, *Thin-Walled Struct.* 44 (2006) 399–406.
- [17] K. Magnucki, M. Rodak, J. Lewiński, Optimization of mono- and anti-symmetrical I-sections of cold-formed thin-walled beams, *Thin-Walled Struct.* 44 (2006) 832–836.
- [18] B.P. Gilbert, L.H. Teh, H. Guan, Self-shape optimisation principles: Optimisation of section capacity for thin-walled profiles, *Thin-Walled Struct.* 60 (2012) 194–204.
- [19] P. Sharafi, L.H. Teh, M.N.S. Hadi, Shape optimization of thin-walled steel sections using graph theory and ACO algorithm, *J. Constr. Steel Res.* 101 (2014) 331–341.
- [20] B.W. Schafer, Review: the direct strength method of cold-formed steel member design, *J. Constr. Steel Res.* 64 (2008) 766–778.
- [21] J.H. Holland, *Adaptation in Natural and Artificial Systems*, University of Michigan Press, Ann Arbor, MI, USA, 1975.
- [22] H. Adeli, N. Cheng, Augmented Lagrangian Genetic Algorithm for structural optimization, *J. Aerosp. Eng.* 7 (1994) 104–118.
- [23] AS/NZS 4600, Cold-formed Steel Structures, Standards Australia, Sydney, 2005.
- [24] Y.K. Cheung, *Finite Strip Method in Structural Analysis*, Elsevier, Amsterdam, Netherlands, 2013.
- [25] B. Schafer, S. Ádány, Buckling analysis of cold-formed steel members using CUFEM: conventional and constrained finite strip methods, in: R.A. LaBoube, W.-W. Yu (Eds.), Proceedings of the Eighteenth International Specialty Conference on Cold-formed Steel Structures, St. Louis, Missouri, USA, 2006, pp. 39–54.
- [26] B. Schafer, *Direct Strength Method (DSM) Design Guide*, American Iron and Steel Institute, Washington, DC, USA, 2006.
- [27] S. Ádány, A.L. Joó, B.W. Schafer, Buckling mode identification of thin-walled members by using cFSM base functions, *Thin-Walled Struct.* 48 (2010) 806–817.
- [28] The Lysaght Referee – 32nd Edition, BlueScope Steel Limited, NSW, Australia, 2009.
- [29] T.J.M. Savoyat, B.P. Gilbert, L.H. Teh, Self-shape Optimisation of Cold-formed Steel Columns, Research Report CIEM/2012/R01, 2012.
- [30] D.R. Griffiths, J.C. Miles, Determining the optimal cross-section of beams, *Adv. Eng. Inform.* 17 (2003) 59–76.
- [31] S.H. Pham, C.H. Pham, G.J. Hancock, Direct strength method of design for shear including sections with longitudinal web stiffeners, *Thin-Walled Struct.* 81 (2014) 19–28.
- [32] C.H. Pham, G.J. Hancock, Direct strength design of cold-formed C-sections for shear and combined actions, *J. Struct. Eng.* 138 (2012) 759–768.